AD-A172 237 UNDERSTANDING THE HIP (HOT ISOSTATIC PRESSING) CONSOLIDATION OF P/M NICKEL-BASE SUPERALLOYS(U) COLUMBIA UNIV NEW YORK J K TIEN 30 APR 86 1/1

UNCLASSIFIED AFOSR-TR-86-0626 AFOSR-82-0352 F/G 11/6 NL

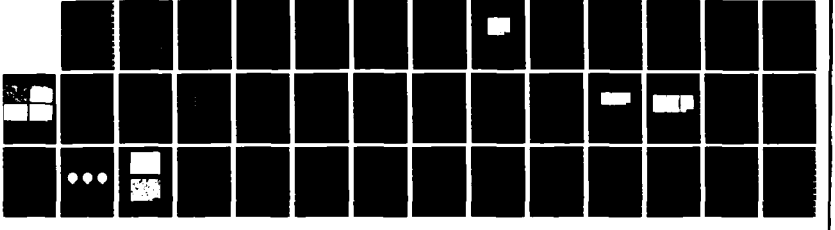

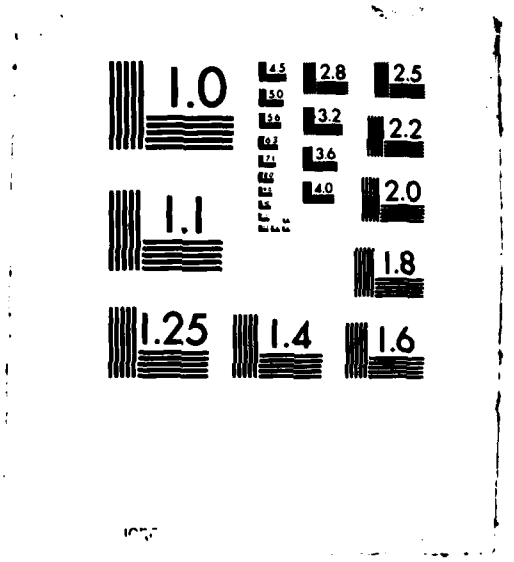
1.0
1.1
1.25
1.4
1.6
1.8
2.0
2.2
2.5
2.8
3.2
3.6
4.0
4.5
5.0
5.6
6.3

UNCLASSIFIED

SECURITY CLASSIFICATION OF THIS PAGE (When Data Entered)

REPORT DOCUMENTATION PAGE		READ INSTRUCTIONS BEFORE COMPLETING FORM
1. REPORT NUMBER AFOSR-TR- 86-0626	2. GOVT ACCESSION NO.	3. RECIPIENT'S CATALOG NUMBER
4. TITLE (and Subtitle) Annual Report for Air Force Grant AFOSR-82-0352A2		5. TYPE OF REPORT & PERIOD COVERED Progress, 10/1/84 - 9/30/85 6. PERFORMING ORG. REPORT NUMBER
7. AUTHOR(s) Prof. John K. Tien		8. CONTRACT OR GRANT NUMBER(s) AFOSR-82-0352A2
9. PERFORMING ORGANIZATION NAME AND ADDRESS Columbia University New York, NY 10027		10. PROGRAM ELEMENT, PROJECT, TASK AREA & WORK UNIT NUMBERS 61102F 2306/A1
11. CONTROLLING OFFICE NAME AND ADDRESS AFOSR/NE BLDG 410 BAFB DC 20332		12. REPORT DATE 4/30/86 13. NUMBER OF PAGES 38
14. MONITORING AGENCY NAME & ADDRESS (if different from Controlling Office) same as 11		15. SECURITY CLASS. (of this report) Unclassified 15a. DECLASSIFICATION/DOWNGRADING SCHEDULE

16. DISTRIBUTION STATEMENT (of this Report)
APPROVED FOR PUBLIC RELEASE, DISTRIBUTION UNLIMITED

17. DISTRIBUTION STATEMENT (of the abstract entered in Block 20, if different from Report)

18. SUPPLEMENTARY NOTES

19. KEY WORDS (Continue on reverse side if necessary and identify by block number)

20. ABSTRACT (Continue on reverse side if necessary and identify by block number)

DD FORM 1 JAN 73 1473 EDITION OF 1 NOV 65 IS OBSOLETE

UNCLASSIFIED

SECURITY CLASSIFICATION OF THIS PAGE (When Data Entered)

AFOSR-TR- 86-0626

SUMMARY PROGRESS REPORT

for

Air Force Grant AFOSR-82-0352A2

Submitted to

Dr. Alan H. Rosenstein

for Research in

"Understanding the HIP Consolidation of P/M Nickel-Base Superalloys"

Period: 1 October 1984 to 30 September 1985 (Year Three)

Table of Contents

I. Executive Abstract

Powder metallurgy is a route often taken in superalloy processing, and hot isostatic pressing (HIP) to near-net shape is the most cost-effective method of superalloy powder consolidation. However, as-HIP superalloys have been plagued by poor mechanical properties, which can be ascribed, ~~to materials~~ cleanliness and to prior particle powder boundaries (PPB). The solution to ~~the first~~ problem is the policing of the process, and the solution to the second problem is more technical and pivots about altering the deformation mechanism comprising HIP densification to minimize PPB.

Previously the mechanisms of densification during HIP have not been well understood. It is thought that, under the commercial temperature and pressure conditions of HIP of superalloy powders, deformation occurs primarily by creep. Since ~~the~~ commercial powder consists of particles of unequal size, a variation in the extent of deformation is seen. ~~The~~ small particles are smeared ~~in~~ between ~~the~~ large particles, which remain relatively undeformed ~~(Figure 1)~~. The undeformed boundaries or PPB are sites for precipitation of blocky gamma prime and deleterious carbides. If deformation of all powder particles could be maximized, PPB would be minimized and a more reliable consolidate would be the result. However, the knowledge of mechanisms and kinetics of HIP is not sufficient to indicate temperature and pressure conditions for uniform maximum deformation of all powder particles.

~~This research program was undertaken~~ to advance ~~the~~ scientific understanding of HIP and to apply that understanding to HIP processing, and demonstrate improved mechanical properties. In Years One through Three of the program, several of our goals set in previous proposals have been met.

In Year One, the argon-atomized Rene 95 powder used in the HIP studies was

completely characterized in terms of surface morphology, porosity, microstructure, and carbon and carbide content. Furthermore, HIP runs were done at one commercial pressure and temperature (1120°C and 103 MPa) for varying hold times (5-180 minutes) and for three different size distribution of powders: monosized (-170 +200), bimodal (80% -170 +200, 20% -400 +500), and full size (-150 mesh). Contrary to industrial belief, densification was nearly instantaneous. Full density was reached even with a hold time of only 5 minutes. The mechanism of deformation at these conditions is mainly athermal plastic flow rather than creep deformation. It was found that the rapid deformation and/or full size powder distribution lead to a greater density of PPB.

Consolidation at atmospheric pressure (CAP) runs were also conducted at two temperatures (1218°C and 1121°C, at .101 MPa) for varying hold times for the full powder size distribution, and experimental densification rate laws have been obtained. At the higher temperature of 1218°C, sintering and grain coarsening are expected to be dominant, since the γ' solvus of Rene 95 is around 1160°C and the solidus is around 1246°C.

In Year Two, in order to promote more uniform densification deformation, i.e., creep, additional HIP runs were done at two conditions of lower pressures and temperatures (900°C, 103 MPa and 1000°C, 10.3 MPa) for varying hold times (5-180 minutes) and for the same three powder size distributions. Experimental densificatioan rate laws have been obtained. No fully dense material was obtained, even after 3 hours hold time. The uniformity of densification was analyzed by PPB morphology.

In the second and third years, high temperature tensile tests were also run on as-HIP Rene 95 to determine the strain rate and temperature regime of superplastic deformation. Calculations are now being done to relate true strain rate to HIP pressure. In addition, more tests, using stepped strain rate

tensile tests, have been performed.

In pace with the experimental work, an analytical model for the mechanisms and kinetics of HIP densification was developed and is now in publication.

Now, at the end of the third year, all HIP and CAP material from Years One and Two has been analyzed in quantitative terms of PPB and powder particle deformation.

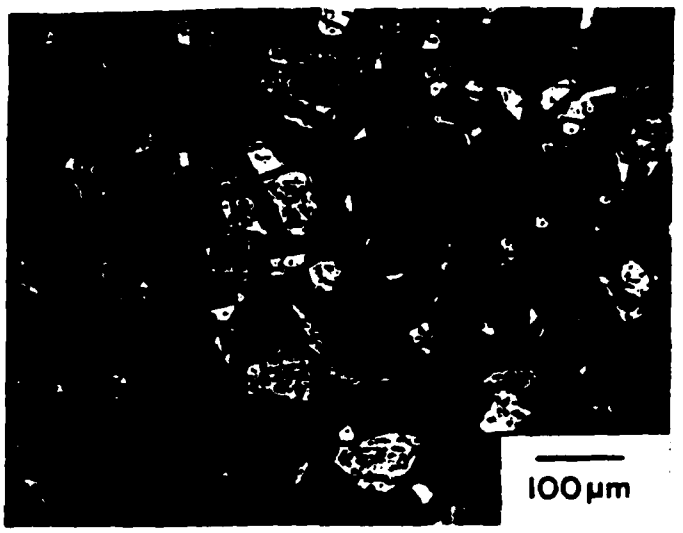

Figure 1. PPB morphology in fully dense Rene 95 consolidated at typically reported HIP conditions (-140 mesh powder, 1120°C, 103 MPa).

II. Progress Report for Year Three

A. Regimes in Pressure and Temperature of the Various Deformation Mechanisms

The mechanisms of deformation in various pressure/temperature regimes were determined by running true strain rate controlled tensile tests at strain rates ranging from 2×10^{-5}/sec to 1×10^{-2}/sec and temperatures of 1000°, 1050°, 1100°, and 1150°C, temperatures in the range where HIP and forging of Rene 95 is done. The strain rate results are indicated in Figure 2 as a log-log plot of the flow stress (σ) versus strain rate (ε). The slope of the curves, that is, the strain rate exponent (m), is plotted in Figure 3 as a function of the strain rate and shows an anticipated peak in the exponent m at the temperatures investigated. The ductility results are shown in Table I with the associated values of m. All values shown are for engineering strain at failure except for those in parentheses, which were tests terminated before failure. Superplasticity is expected to dominate the deformation behavior at the peak ($m > .3$) although relatively large ductilities (indicating some superplastic behavior) was obtained even at off-peak values of m ($m < .2$), i.e., at 1150°C and 1×10^{-4}/sec, $m = .19$ although the ductility was 148 percent. This appears to be due to grain coarsening (Figure 4), especially since 1150°C is above the γ' solvus. We also found evidence of low ductility (40 percent) at close to peak value of m at the temperature of 1100°C, and we believe that prior particle boundaries may inhibit superplastic deformation by offering sites for crack nucleation especially at the higher stress regimes and higher strain rates. Thus optimal superplastic behavior in terms of ductility is obtained at lower temperatures and when the peak value of m is reached at lower strain rates. Microstructural analysis has been done to confirm this hypothesis.

Table I.

	$2x10^{-5}$	m	$1x10^{-4}$	m	$1x10^{-3}$	m	$3x10^{-3}$	m	$1x10^{-2}$
1000°C	(240%)	.46	239%						
1050°C	(234%)	.45	515%	.49	160%	.40	60%		
1100°C	(190%)	.22	445%	.38	160%	.46	72%	.35	35%
1150°C			148%	.16	60%	.37	40%	.33	40%

To further elucidate the deformation mechanisms, the activation energy (Q) for the deformation at various values of stress was found and the results of Q versus σ are shown in Figure 5 along with literature values of Q for various mechanisms for the purposes of comparison. Consistent with our analysis, superplastic behavior appears to be favored at intermediate stresses. If the stresses are too low, diffusion is favored whereas at high stresses a transition appears to occur to a power law creep mode. We believe that the regime of superplastic behavior can be further extended by limiting PPB formation, particularly for the lower temperature HIP runs for which the creep stresses are relatively high.

In order to more fully investigate the superplastic behavior of Rene 95, stepped strain rate tension tests (Figure 6) were used (initially to conserve material). However we found that the flow stress of the material was path dependent on the strain rates at the temperature investigated, and m could not be validly determined (Figure 7). Further invesigation into this effect showed that another aerospace material, Ti-17, was indeed strain rate path independent at temperatures typically used for forging of the material, for

stepped strain rate tests in compression (Figure 8). The titanium alloy is probably path independent due to the lack of work hardening, as can be seem in the very flat σ-ε curve at these temperatures, particularily since the forging temperature for Ti-17 is relatively high compared to the melting temperature of the material. Rene 95 is isothermally forged below the γ' solvus temperature to prevent excessive grain growth, and the material undergoes work hardening. These results have some impact in forging, because tensile and compression tests are used as input for predictive forging modeling, and for some cases, the forging process may not be accurately represented by single strain rate tensile or compression tests.

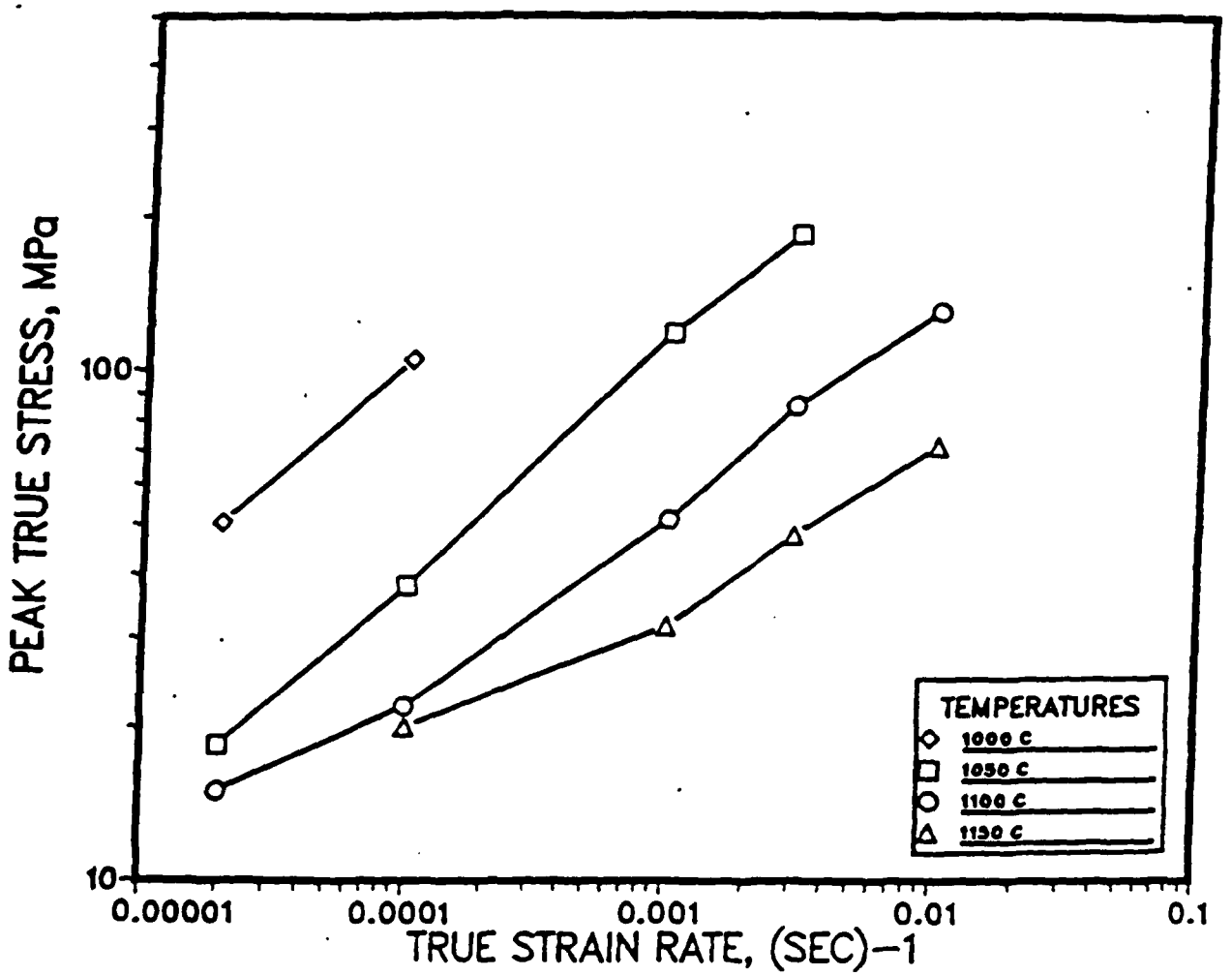

Figure 2. Peak true stress versus true strain rate, for Rene 95 at several temperatures.

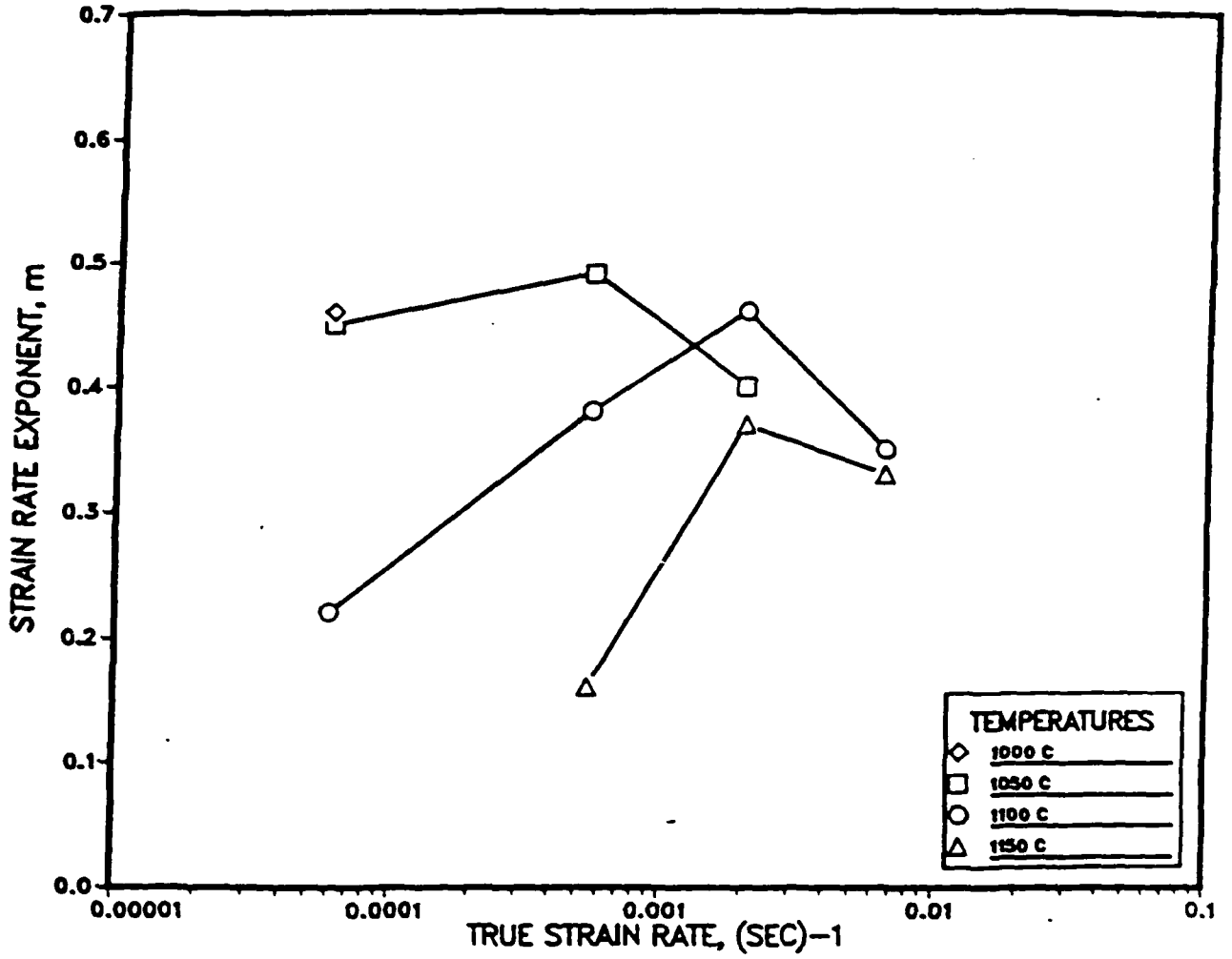

Figure 3. Strain rate exponent (m) versus true strain rate for Rene 95 for several temperatures. Generally, superplastic behavior occurs at m > .3.

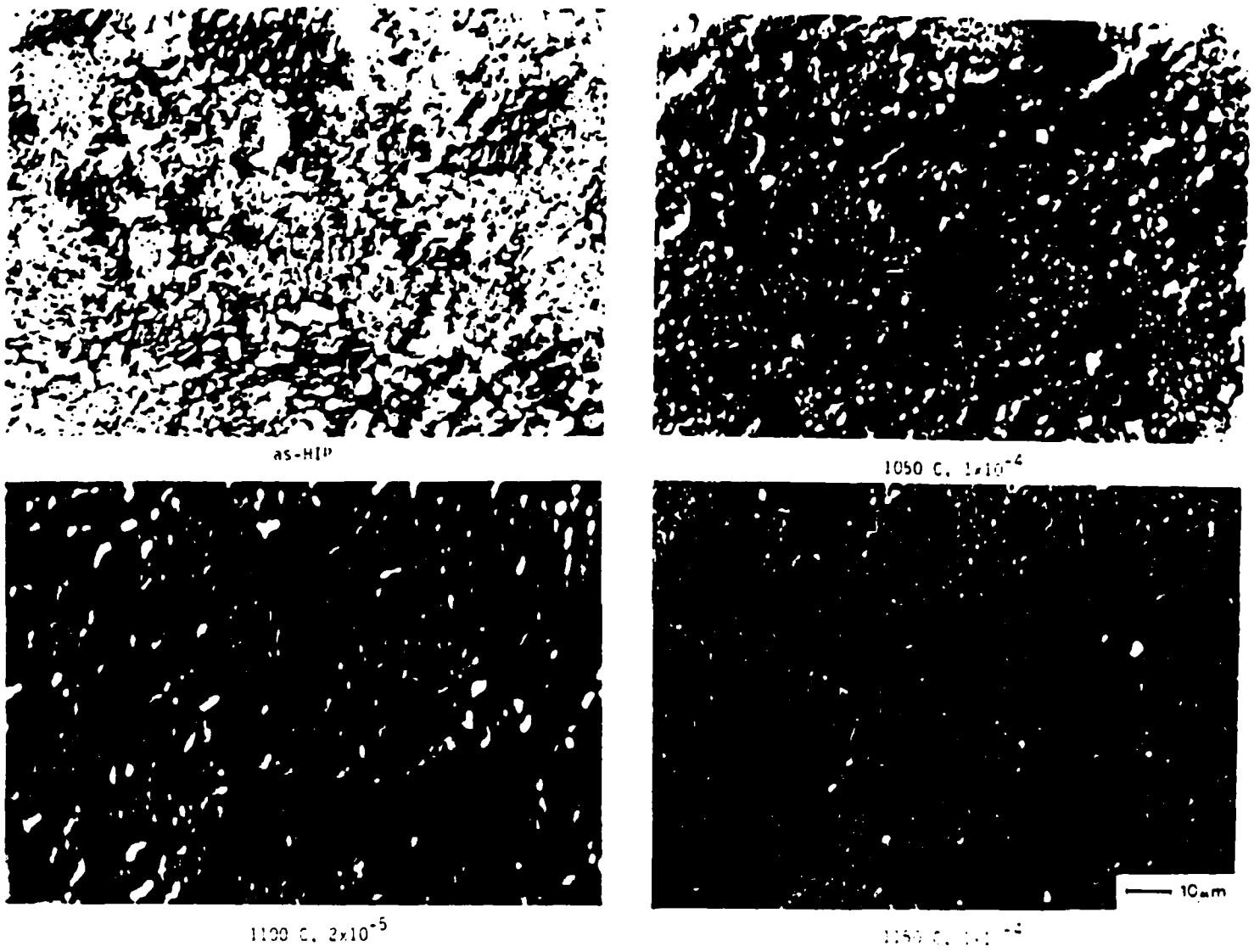

Figure 4. Rene 95 tested at 1150°C, $\dot{\varepsilon} = 1 \times 10^{-4}$, showing grain coarsening and cavitation.

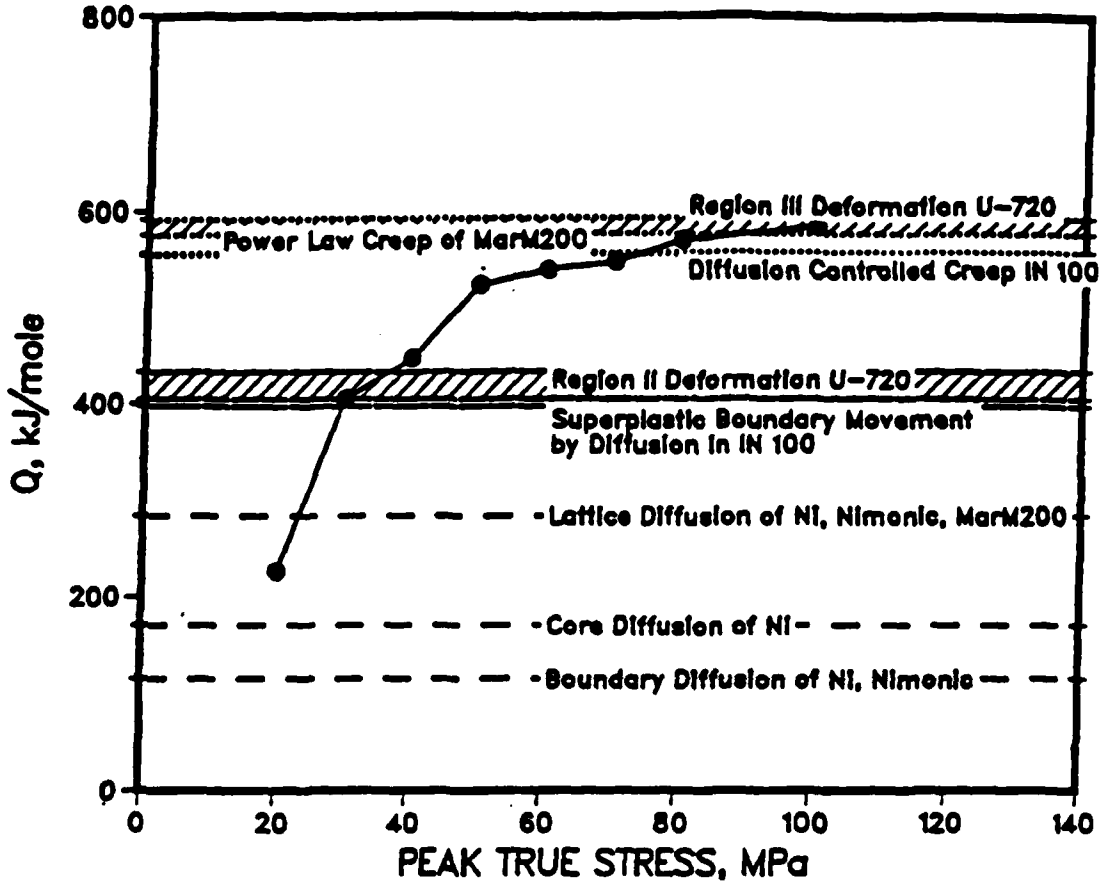

Figure 5. Activation energy versus peak true stress. Note the transition from diffusion to power law creep.

TEST MATRIX

$\dot{\varepsilon}$ (sec^{-1})	926.6°C (1700°F)	898.9°C (1650°F)	871.1°C (1600°F)
1×10^{-5}	10%		10%
1×10^{-4}	10% 10%	10% 10%	10% 10%
1×10^{-3}	60% 10% 10% 10%	60% 10% 10% 10%	60% 10% 10% 10%
1×10^{-2}	60% 10% 10% 30%	60% 10% 10% 10%	60% 10% 10% 30%
1×10^{-1}	60% 10% 30%	60% 10% 30% 30%	60% 10% 30%
1×10^{0}	60% 30%	60% 30%	60% 30%

Engineering Strain at Strain Rate

- Temperature straddles forging and die cooling temperatures

Figure 6. Schematic of a stepped strain rate test. There is a 10% ε dwell at each strain rate.

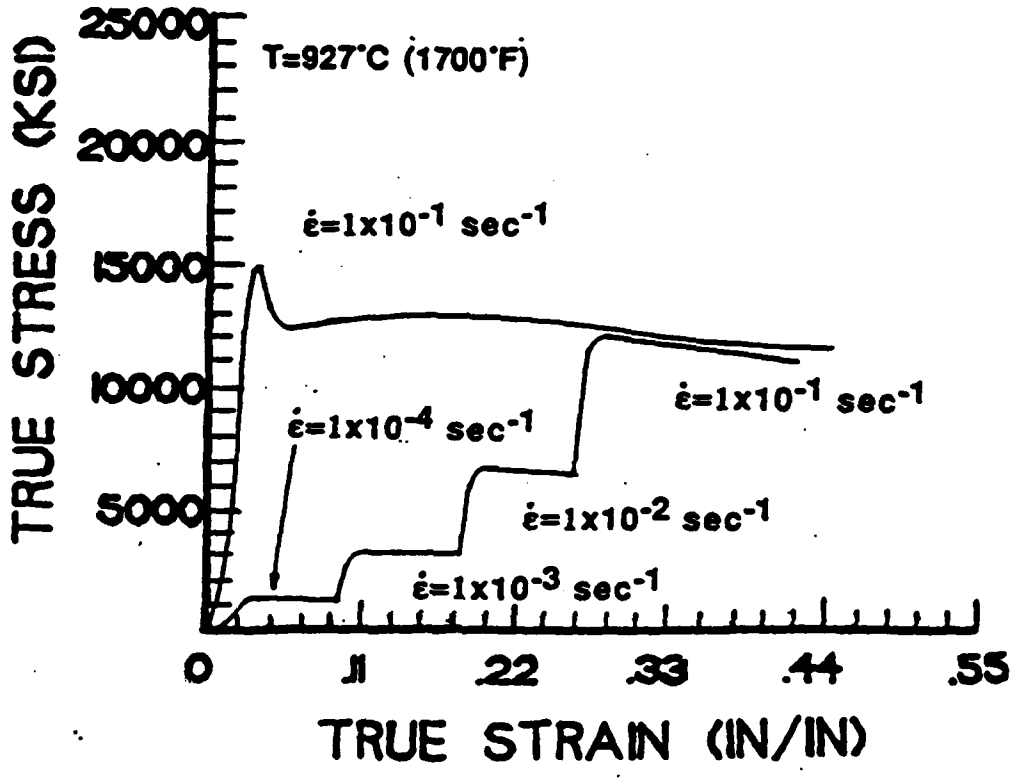

Figure 7. Single and stepped strain rate compression tests for Ti-17.

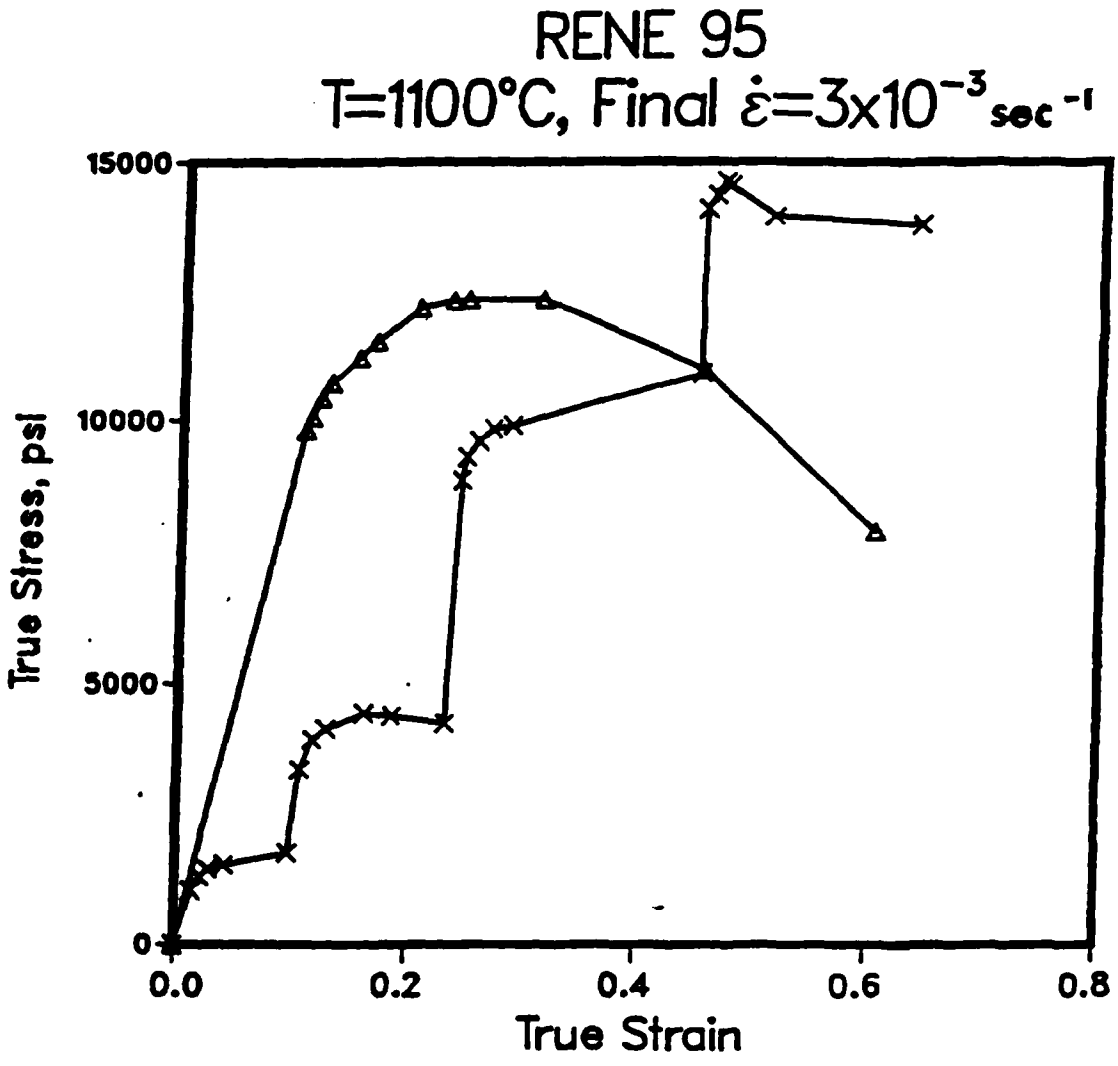

Figure 8. Single and stepped strain rate tensile tests for Rene 95. Note the difference in flow stress for the same strain rate.

B. Influence of Particle Size Distribution and HIP Conditions on HIP Densification

The kinetics of powder densification and powder morphological changes were determined initially at one commercial pressure (P) and temperature (T) condition of 1120°C and 103 MPa for the nickel base superalloy Rene 95. It was found (a surprising fact to the relevant industry) that consolidation for all the particle distribution cases occurred very rapidly (full density reached in 5 minutes, see Table II), mainly by instantaneous plastic flow instead of by local creep deformation. It was also found that non-creep deformation and/or a full distribution of particle sizes can result in a greater number of undeformed particles in the consolidates. The boundaries of these undeformed particles can become prior particle boundaries (PPB). For example, see Figure 9 showing minimum PPB for the monosized case and maximum for the full size distribution.

Table II. Percentage of Full Density, Year One HIP Runs

			% Full Density (100% = 8.290 g/cm³)					
Powder			Hold Time, min					
Distribution	T, °C	P, MPa	5	15	30	60	110	180
Full	1120	103.0	100	100	-	100	-	100
Bimodal	1120	103.0	100	100	100	100	100	100
Monosized	1120	103.0	100	100	100	100	100	100
Full	1120	10.3	92.6	96.5	-	-	-	99.6

At the lower pressure of 10.3 MPa, densification was somewhat less rapid (see Table II), and there was clear evidence (see Figure 10) that the smaller particles underwent the greater proportion of plastic deformation during the HIPing process.

To obtain clear kinetic data, CAP (1 atmosphere, 0.101 MPa) densification on a full size distribution was conducted at two temperatures of 1218°C and 1121°C, and the densification results from these tests are shown in Table III. Clearly, the densification, as expected, is much slower under CAP pressure conditions than at the commercial pressure conditions. The densification mechanism and microstructural evaluation of the CAP specimens are presently underway.

Table III. Percentage of Full Density, CAP

			% Full Density (100% = 8.290 g/cm³)					
Powder			Hold Time, min					
Distribution	T, °C	P, MPa	5	15	60	180	420	960
Full	1218	0.101	66.2	69.8	77.8	90.8	94.0	99.0
Full	1121	0.101	63.9	69.0	67.5	71.4	74.9	78.0

In Years Two and Three, HIP densification was conducted at three lower temperatures and pressures (800°C, 103 MPa; 900°C, 103 MPa and 1000°C, 10.3 MPa) for all three size distribution cases. The densification results (Table IV) indicate relatively slower densification as with CAP, and powder particles are probably undergoing creep and/or superplastic deformation.

Table IV. Percentage of Full Density, Year Two HIP Runs

			% Full Density (100% = 8.290 g/cm³)			
Powder			Hold Time, min			
Distribution	T, °C	P, MPa	5	15	60	180
Full	800	103.0	-	-	76.1	-
Full	900	103.0	79.1	81.6	84.2	89.4
Full	1000	10.3	75.7	77.3	80.4	85.2
Bimodal	1000	10.3	75.0	77.2	85.1	91.4
Monosized	1000	10.3	71.6	79.6	81.1	85.2

Figures 11, 12, and 13 show the effect on kinetics of temperature, pressure, and powder size distribution, respectively. The vertical dotted line represents the four hour hold time, as is generally reported for HIP of Rene 95 in the literature. Lowering either the temperature or the pressure slows the densification rate, however temperature (at least at 103 MPa) has a greater influence on the kinetics. For only a 200°C drop in temperature, densification is slowed to the point that none of the HIP runs reached full density in four hours (Figure 11), but an order of magnitude drop in pressure still yields fully dense material within four hours (Figure 12). In Figure 12, the difference in consolidation mechanism for CAP is clearly seen by the concave shape of the densification curve. The powder size distribution appears to have only a small effect, due mainly to the difference in initial powder densities. This small effect even lessens as densification progresses.

The deformation of individual powder particles in the not-fully dense material is difficult to judge, however, looking at the curvature of the

boundary between two particles in a bimodal distribution gives a qualitative picture of particle deformation. Three cases exist - the boundary may deflect toward the small particle, the large particle, or the boundary may be even between the two particles (Figure 14). The initial curvature of the boundary gives an indication of which particle will deform more as densification proceeds. By looking at the relative number of each type of boundary, the uniformity of deformation can be determined. Figure 15 shows the microstructure of material from two different HIP runs - both are bimodal powder distributions. Figure 15(a) shows material consolidated at 1120°C, 103 MPa, and Figure 15(b) shows material consolidated at 1000°C and 10.3 MPa. Table V shows the relative number of contacts for the two HIP conditions. It is clearly seen that the lower temperature and pressure HIP leads to more uniform deformation. This is probably due to the change in deformation mechanism operational during consolidation.

Table V. Relative Number of Each Type of Boundary.

	Relative Percentage of Contacts	
Deforming Particle	1120°C	1000°C
Small	44%	31%
Large	20%	36%
Equal	36%	33%

In light of the densification kinetics obtained from HIP runs of Years One and Two, the HIP conditions for Year Three/Four HIP runs have been chosen. Larger scale (30 lb. cans) are being produced, of full and monosized powder

distributions. The lead time is especially long for this large quantity of monosized powder, and the powder is scheduled to be available Spring 1986. HIP conditions have been tenatively chosen (Table VI) to achieve full density at lower temperatures and pressures, with two cans at the baseline 1120°C, 103 MPa condition.

Table VI. Year Three/Four HIP Run Conditions (tenative).

Powder Distribution	T, °C	P, MPa	t, hrs
Full and Monosized	1120	103	4
Full and Monosized	1100	10.3	4
Full and Monosized	1000	103	4
Full and Monosized	1000	50	8
Full and Monosized	950	103	8

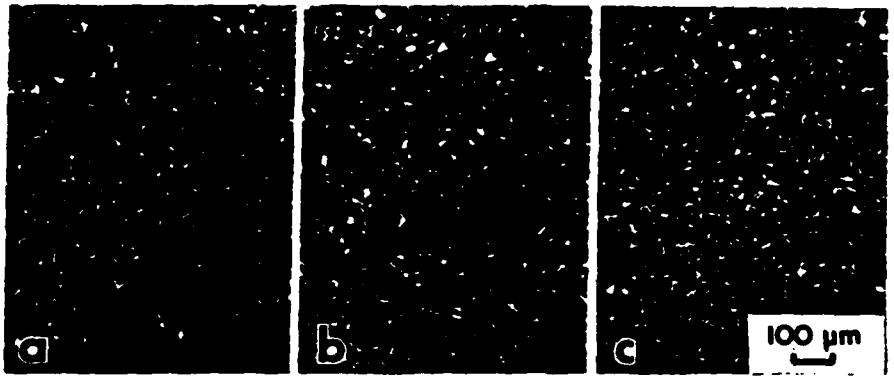

Figure 9. Optical micrographs of HIP Rene 95 powder after a five minute hold time at 1120°C and 103 MPa for a) monosized, b) bimodal, and c) full sized powder distributions.

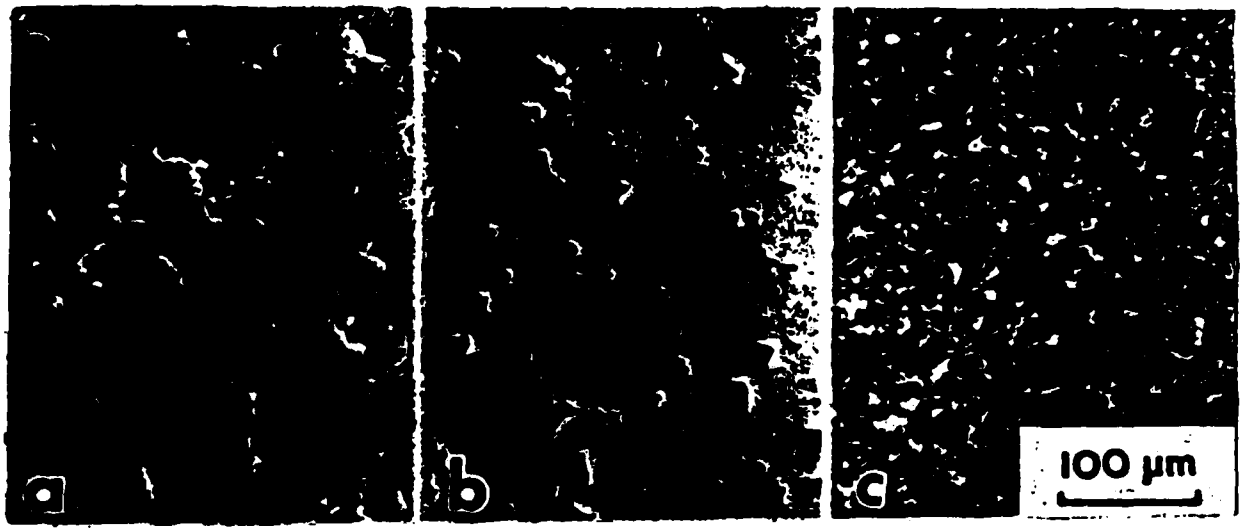

Figure 10. Optical micrographs of HIP Rene 95 powders (full sized distribution) showing morphological changes of powders as a function of hold time at 1120°C and 10.3 MPa: a) 5 minutes, b) 15 minutes, c) 60 minutes.

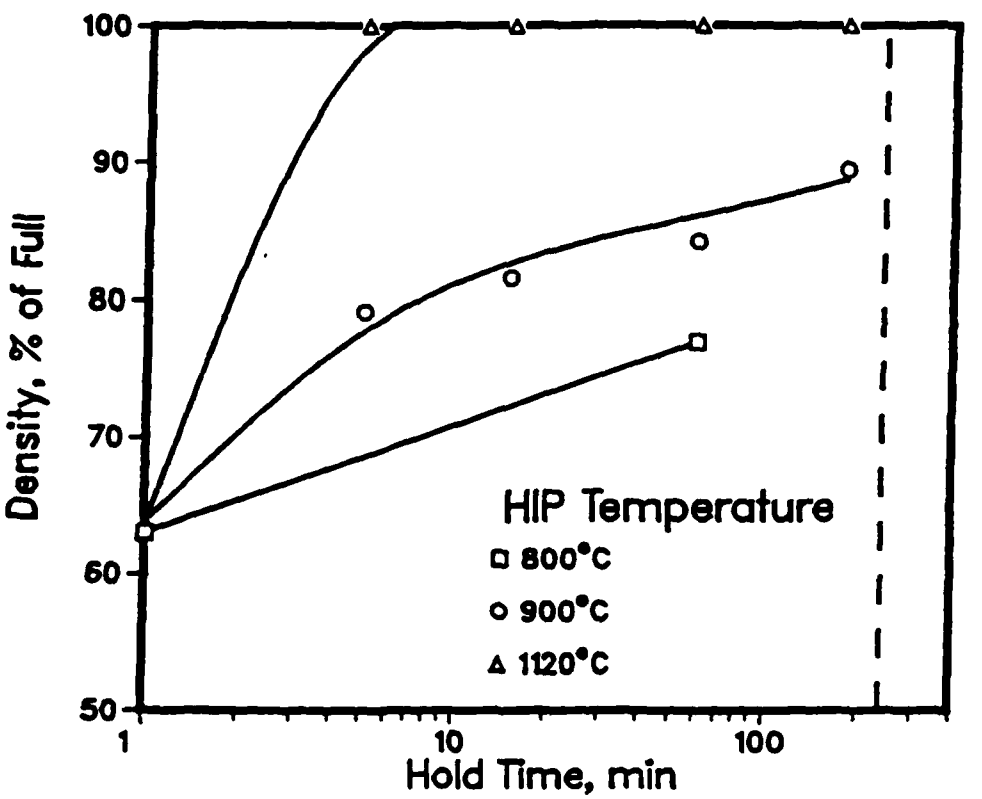

Figure 11. Effect of temperature on kinetics of full sized Rene 95 powder at 103 MPa.

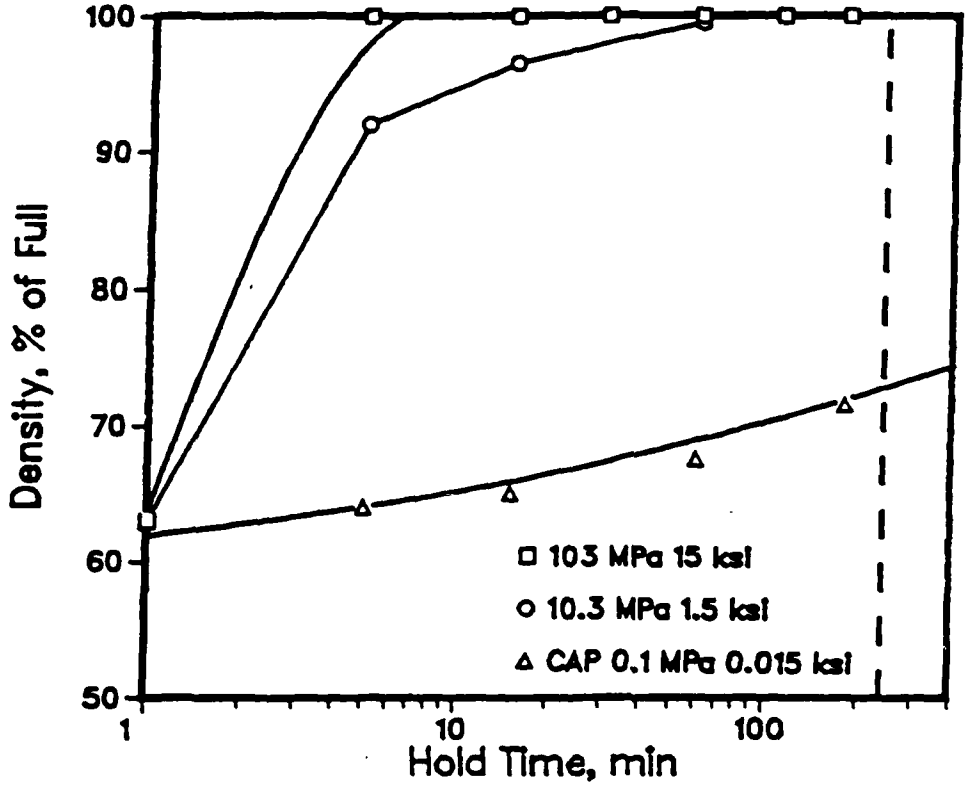

Figure 12. Effect of pressure on kinetics of full sized Rene 95 powder at 1120°C.

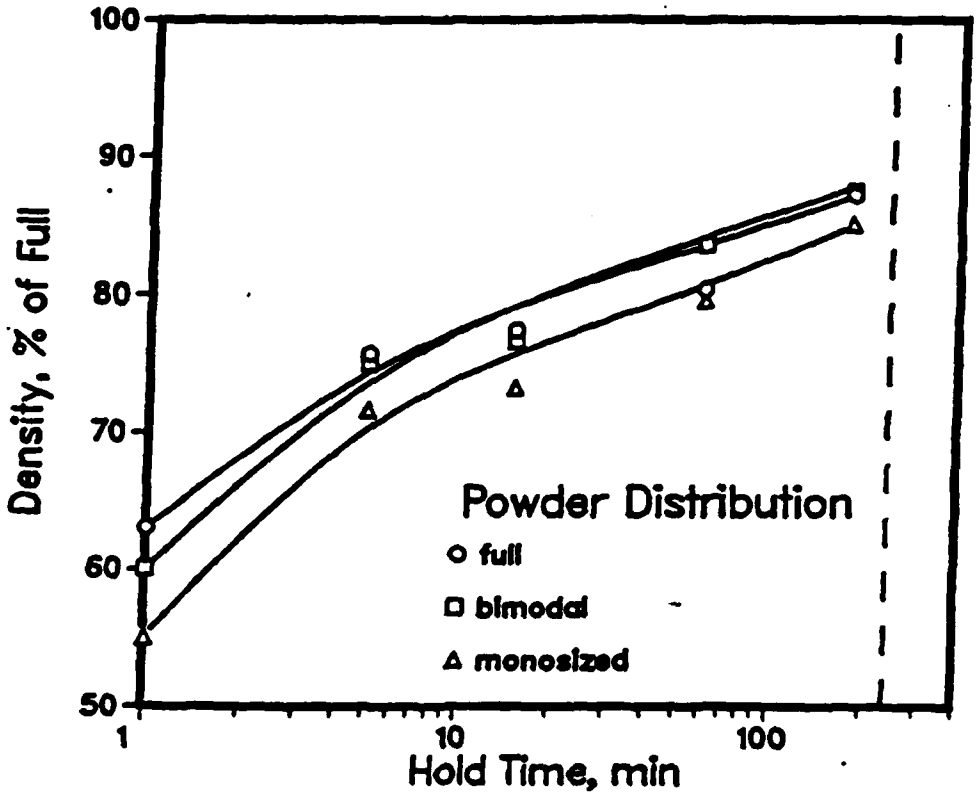

Figure 13. Effect of powder distribution on kinetics of Rene 95 powder at 1000°C and 10.3 MPa.

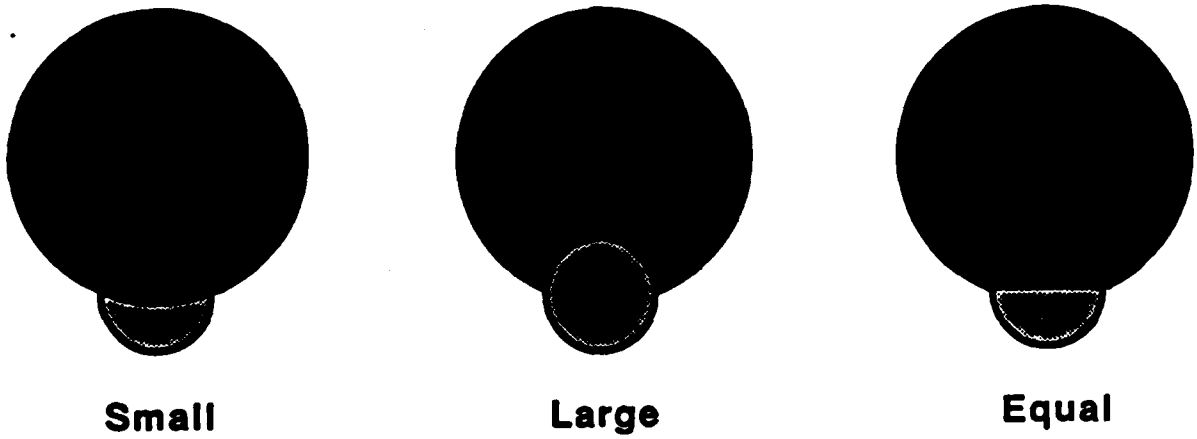

Figure 14. Curvature of particle boundaries showing the three cases of powder particle deformation.

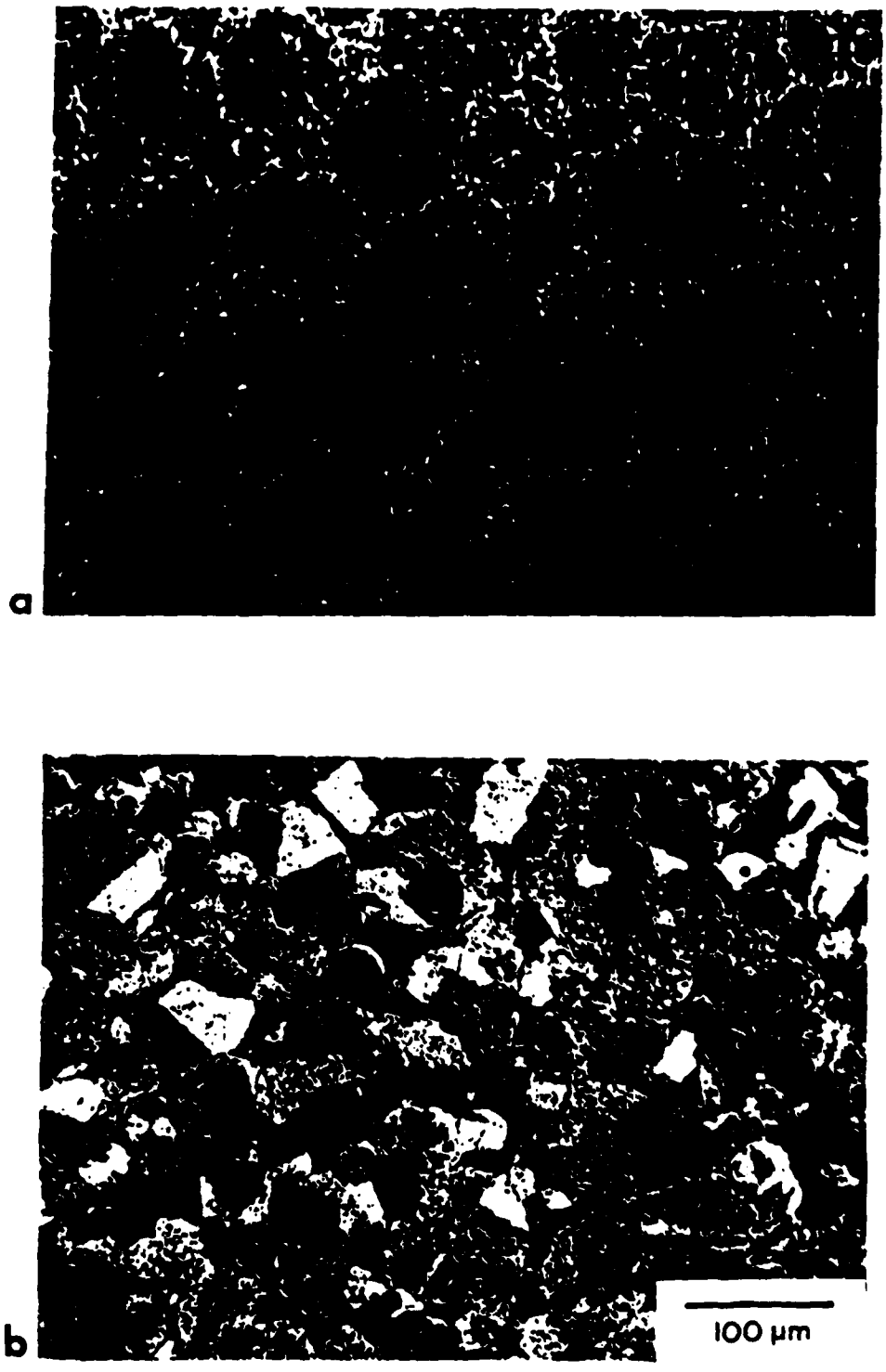

Figure 15. Bimodal Rene 95 powder HIPed at a) 1120°C, 103 MPa, 3 hrs.; b) 1000°C, 10.3 MPa, 3 hrs.

C. Analytical Model for HIP Densification

Previous modeling of densification kinetics by Arzt, Ashby, and Easterling considers only a single particle size. However, in reality P/M consolidates are made of a natural distribution of powder sizes below a given mesh size. The possible disparity between theory and practice has prompted the development of a new model to incorporate the influence of a particle size distribution on both the kinetics of HIP densification and the deformation mechanisms operating during HIP consolidation of superalloy powders. This is done for a more realistic bimodal (or two size) distribution of powders. In order to rederive the HIP densification mechanism map for a bimodal particle distribution, expressions are derived for (a) the distribution of unequal sized particles in a random mixture, and (b) the relationship between the interparticle contact force and the applied pressure.

The radial distribution of powder particles in a bimodal distribution was also experimentally determined by point counting on sections of powder mounted in plastic. Figure 16 shows the results as (N_{ij}), the number of particles of size j around a particle of size i, as a function of radial distance normalized to the radius of the small particles (i,j = 1). The large particles are denoted as i,j = 2.

The results of (a) are obtained in open form using the Percus-Yevik hard sphere approximation for the molecular structure of liquid alloys as derived by J.L. Lebowitz, namely,

$$rg_{ij}(r) = (1/2\pi i) \int_{\delta-i}^{\delta+i} 12(n_i n_j) G_{ij}(s) \exp(sr)\, ds \qquad (1)$$

where $g_{ij}(r)$ is the radial distribution function between the i^{th} and j^{th} particle, $n_i = \pi\rho_i/6$ where ρ_i is the density of the i-type atom in nos./unit volume. G_{ij}, which is the number of atoms at any given distance, r, from a central atom and in a thin shell of thickness, dr, is given by

$$G_{ij}(r) = \rho_j 4\pi r^2 g_{ij}(r)\, dr \tag{2}$$

To relate the applied stress, σ_{app}, to the interparticle contact force, F, the relationship for the single size case was modified for the bimodal case to give

$$\sigma_{app} = (F/4\pi)\,[(1-\varepsilon-f_2)G_{12}/r_2^2 + (1-\varepsilon-f_1)G_{12}/r_2^2 + (1-\varepsilon-f_2)G_{11}/r_1^2 + (1-\varepsilon-f_1)G_{22}/r_2^2] \tag{3}$$

where ε is the void volume fraction, f_1 and f_2 the volume fractions of the two different sized particles with respective radii r_1 and r_2, G_{11}, G_{12}, and G_{22} are the coordination numbers 11, 12, and 22, respectively.

Given the above new formulations described by Eqs. (1), (2), and (3), the new model then proceeds to derive for the bimodal case the density as a function of time using the premise that the densification can be modeled by a fictitious growth of the particles around their centers, with the equations involved here being those of mass balance and geometry.

The final results of the theory are shown in Figures 17 - 20. It is interesting (see Figure 17) that the interparticle deviatoric stress causing particle deformation is of the order of 0.1 to as high as 100 times the HIP pressure depending on the particle size and the instantaneous density. Further, this deviatoric stress on the smaller particle can be of the order of 1.5 times that on the larger particle. In addition, Figure 18 indicates that the smaller particles undergo the greater degree of plastic deformation relative to their larger counterparts. These results are in contrast to the Arzt et al. model wherein all particles experience the same levels of stress and strain.

As mentioned (see Figure 10), the smaller particles in a distribution of particles undergo the greater degree of plastic deformation. The theoretical result (see Figures 19 and 20) is even consistent with this finding. Figure 18 predicts, for example, that as both the size and number of smaller particles decrease, the width of the hatched region appears to increase and so does the athermal plastic flow regime in the HIP densification mechanism map.

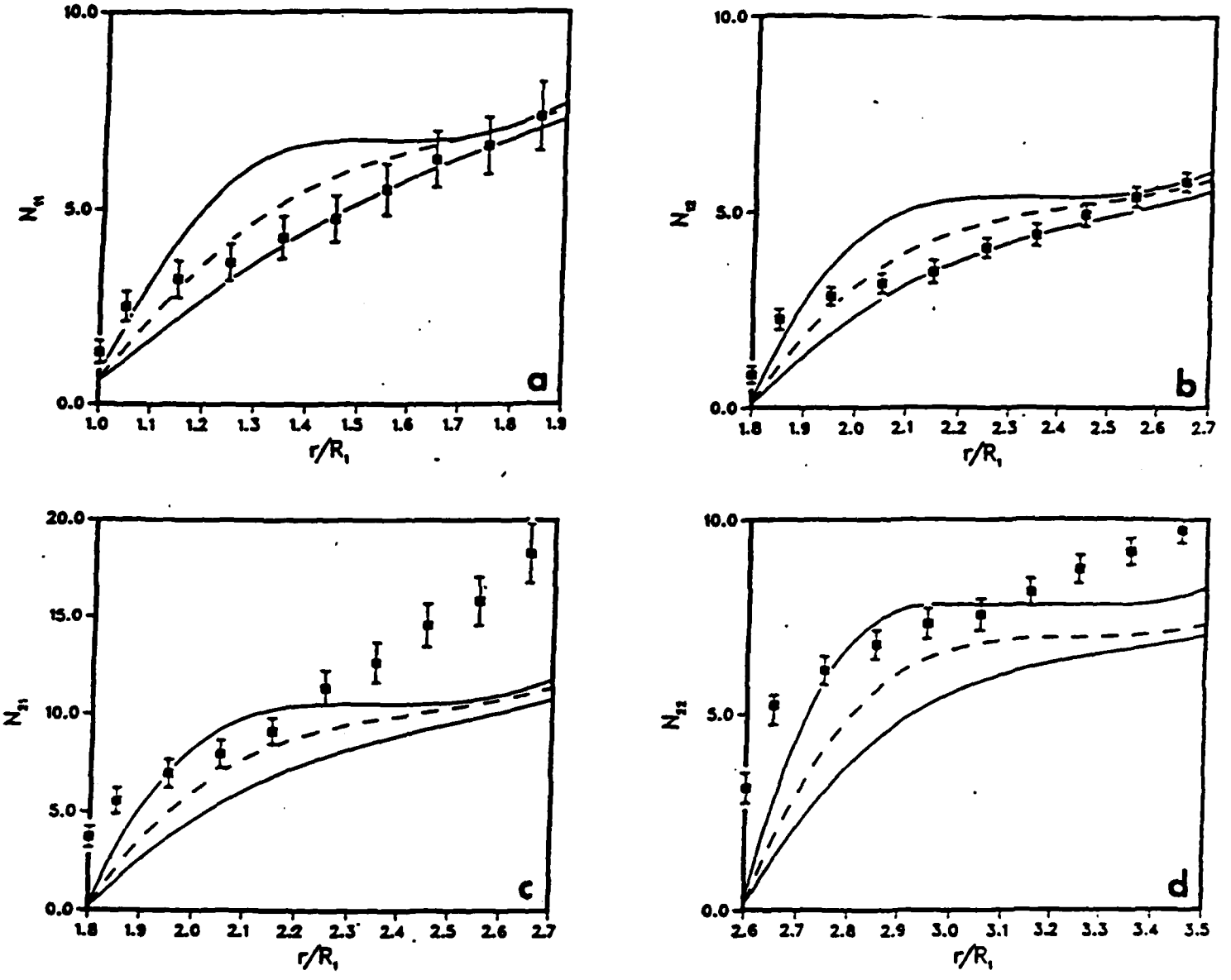

Figure 16. Results of the distribution N_{ij} for the bimodal case with 10% small particles. The solid points are the experimental data points. The lower solid theoretical curve in a) through d) is for $D_e = 0.557$ and the upper solid theoretical curve is for $D_e = 0.671$, the measured upper and lower bounds for D_e (the initial powder density). The dashed curve is the analytical result for the average relative density value of 0.61. All radial distances are normalized to the small particle diameter R_1.

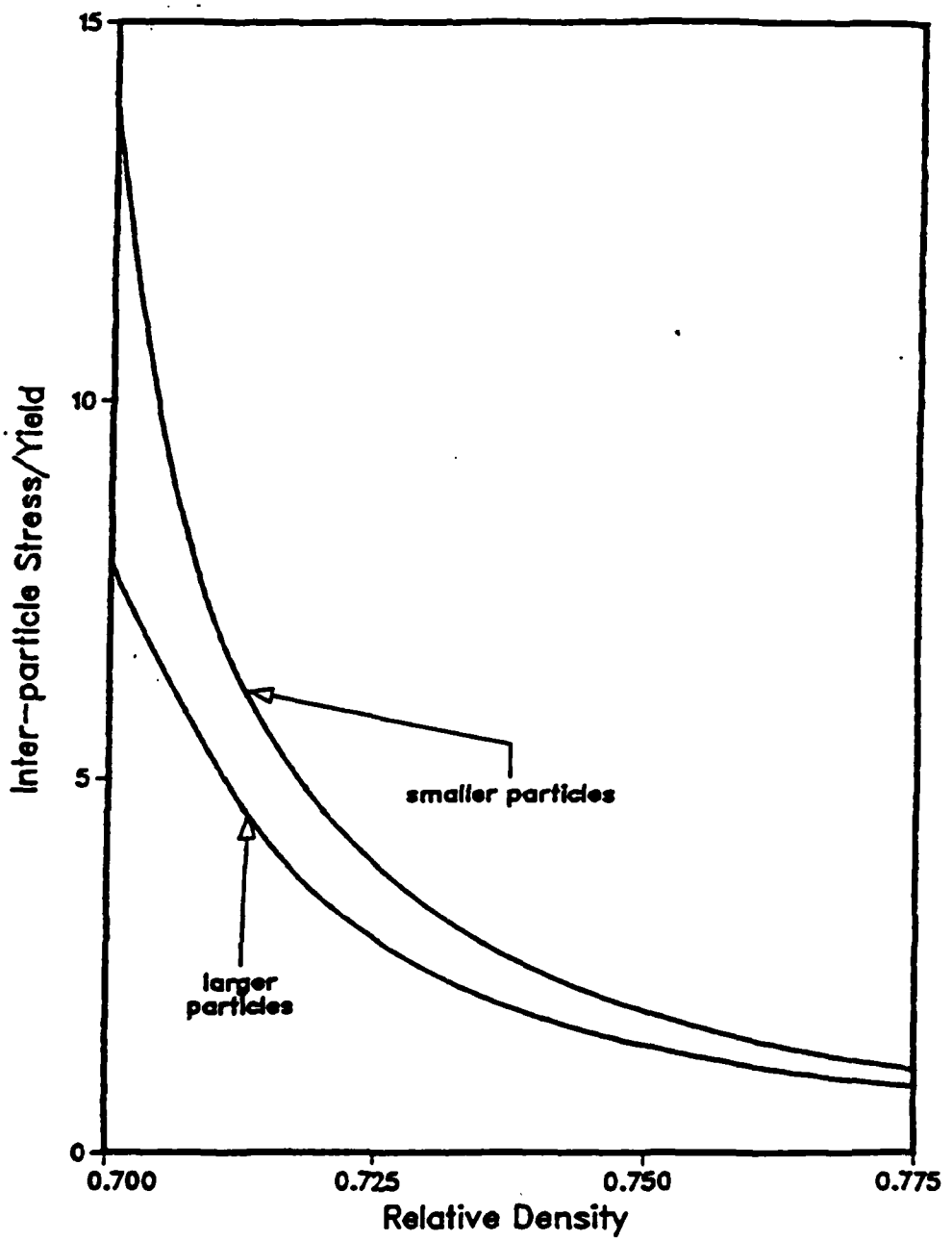

Figure 17. Interparticle contact stresses experienced by smaller and larger particles during HIP of a bimodal size distribution of powders as calculated by Nair and Tien. [log (P/Y) = -1.0, T = 1120°C].

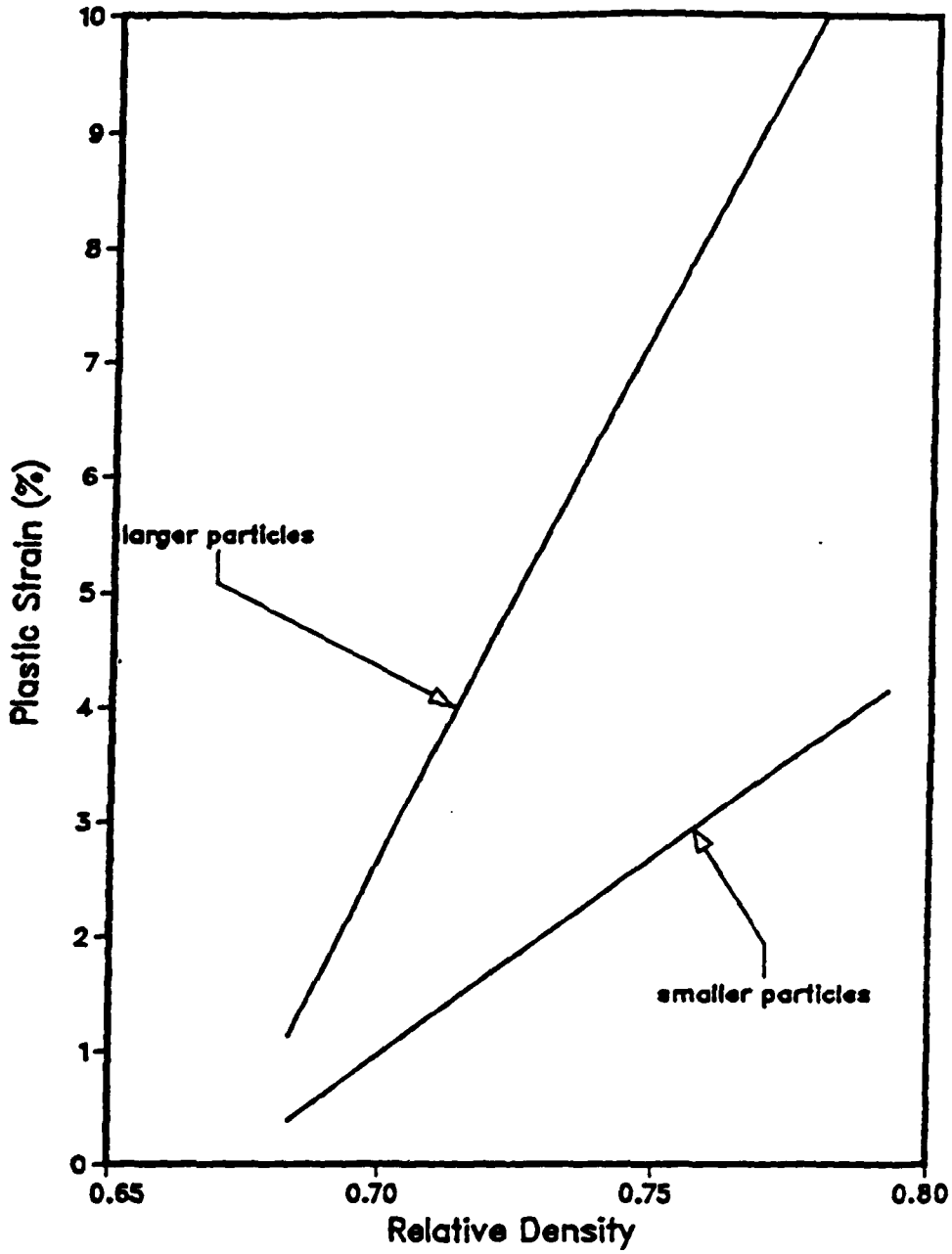

Figure 18. Plastic strain suffered by smaller and larger particles during HIP of a bimodal particle size distribution of powders as calculated by Nair and Tien. [log (P/Y)] = -1.0, T = 1120°C].

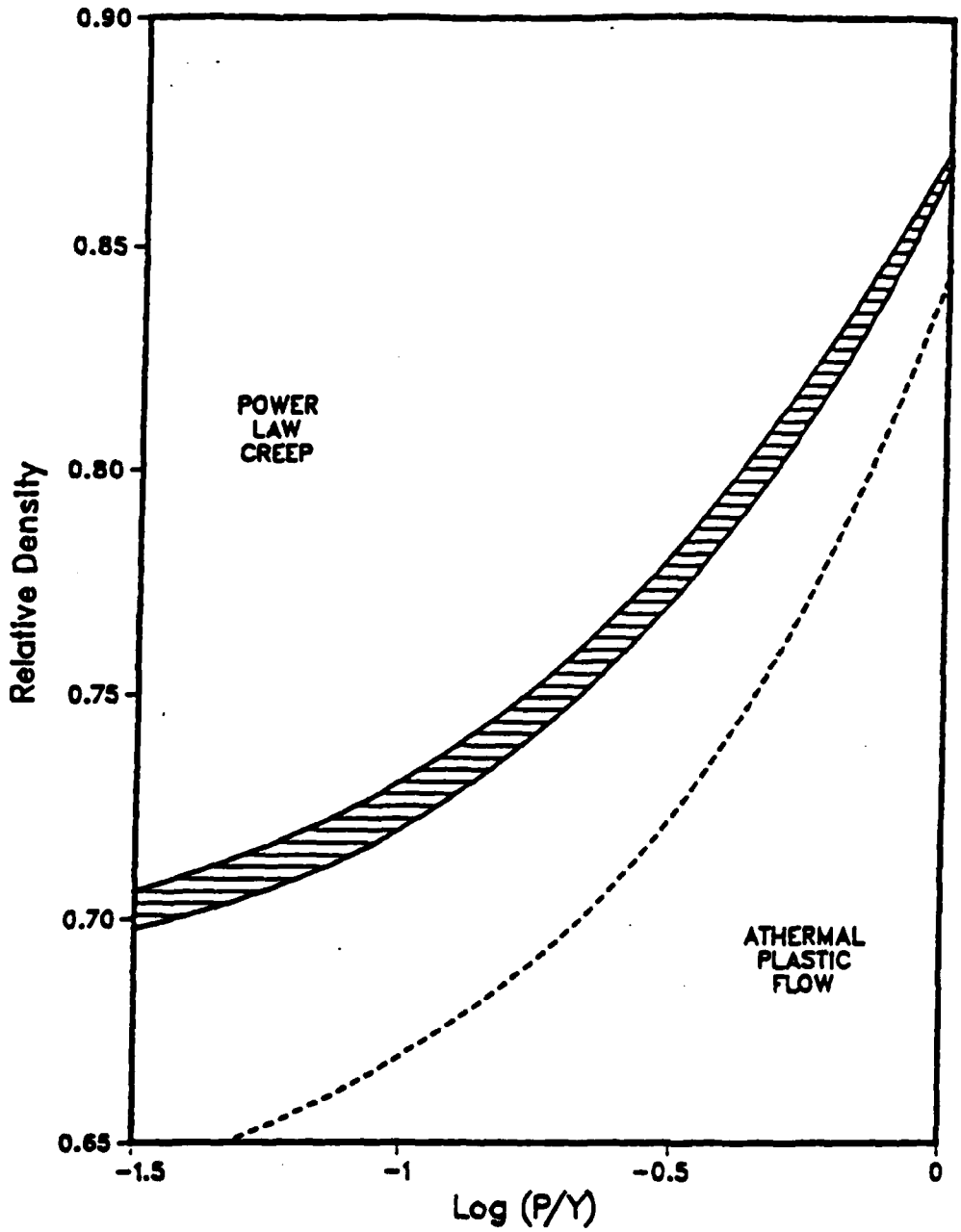

Figure 19. Boundary between the power-law creep and athermal plastic flow regions in a HIP densification map. The dashed line is as calculated by Arzt et al. for deformation of single sized particles. The upper solid line is for the smaller particles and the lower solid line is for the larger particles as calculated by Nair and Tien. [T = 1120°C, particle size ratio = 2.3, and weight percent of smaller particles is 20%].

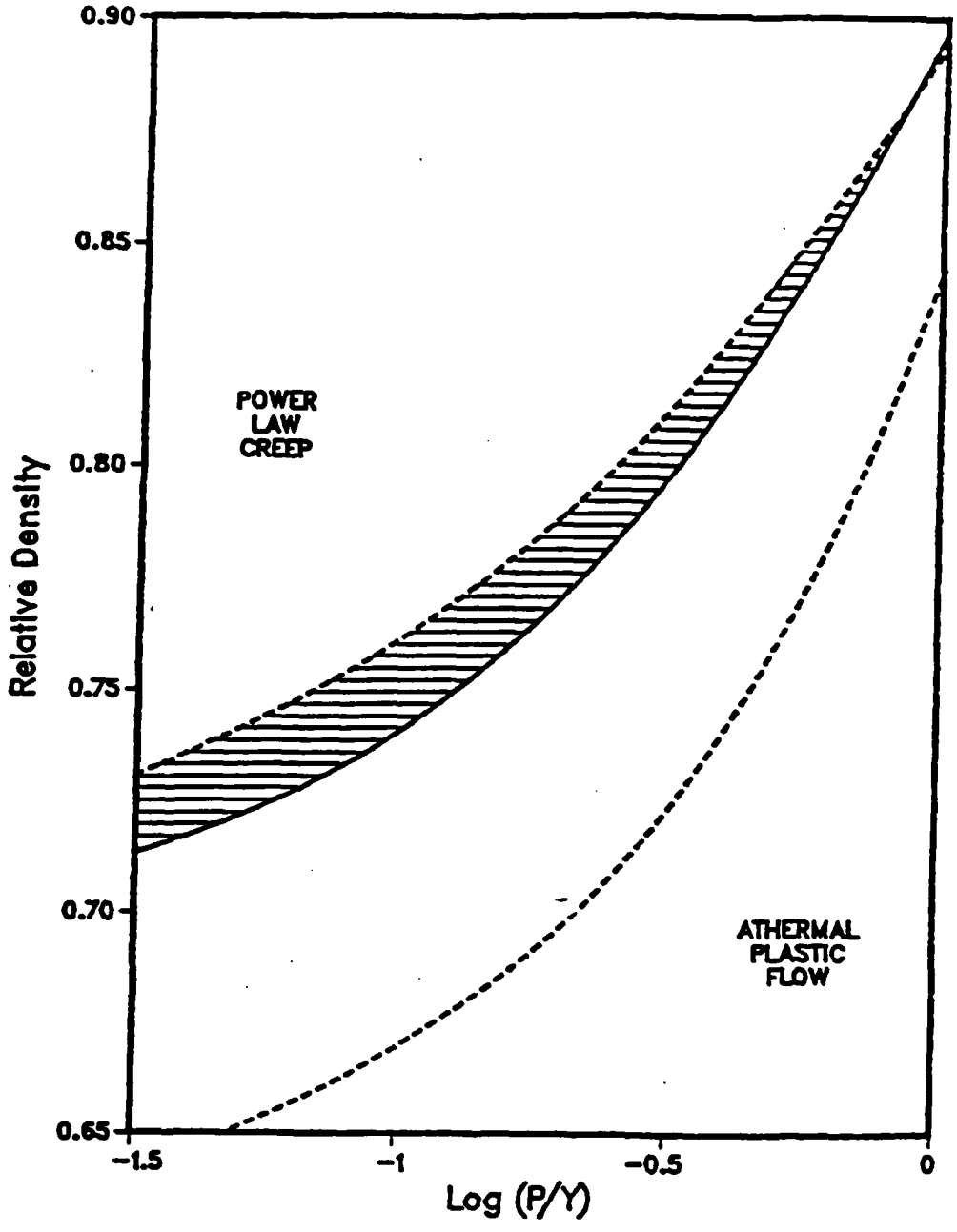

Figure 20. Same as Figure 19 except that the particle size ratio = 4.0 and the weight percent of the smaller particles is 5%.

III. Theses from this Research

Bachelor's Degree:

Choon Ho Lee - September 1980
Brian Hendrix - January 1985
Sharon Ventura - May 1986

Master's Degree:

Barbara Naylor - May 1982
Robert D. Kissinger - September 1980
Janine C. Borofka - May 1985
Theerayuth Lertsirungsun - May 1986

Doctoral Degree:

Robert D. Kissinger - ''Influence of Powder Particle Size Distribution and Pressure on the Kinetics of Hot Isostatic Pressing (HIP) Consolidation of P/M Superalloy Rene 95'' - to be defended.

Janine C. Borofka - ''Deformation Mechanisms and Kinetics in HIP Consolidation of a P/M Superalloy'' - in progress.

IV. Publications and Presentations from this Research

A. Publications

"Powder Metallurgy Superalloys," J.K. Tien, J.C. Borofka, and R.D. Kissinger, Chapter in Rapid Solidification: Materials, Processing, and Applications, ed. B. Cantor, to be published by North Holland.

"Obtaining the Radial Distribution of Random Dense Packed Hard Spheres," S.V. Nair, B.C. Hendrix, and J.K. Tien, accepted for publication in Acta Met.

"Densification Mechanism Maps for Hot Isostatic Pressing (HIP) of Unequal Sized Particles," S.V. Nair and J.K. Tien, accepted for publication in Met. Trans. A.

"Hot Isostatic Consolidation of P/M Superalloys," R.D. Kissinger, S.V. Nair, and J.K. Tien, Proc. 1983 MRS Symposium on Rapidly Solidified Metastable Materials, eds. B.H. Kear and B.C. Giessen, Elsevier Science Publishing, New York, 1984.

"Influence of Powder Size Distribution and Pressure on Kinetics of HIP Consolidation of P/M Superalloy Rene 95," R.D. Kissinger, S.V. Nair, and J.K. Tien, Superalloys 1984, eds. M. Gell et al., AIME Press, Warrendale, PA, 1984.

"Consolidation Science of P/M Superalloys," J.K. Tien and R.D. Kissinger, Proceedings of the 1984 International Powder Metallurgy Conference, Toronto, June 1984, APMI, Princeton.

"Interpretive Review of Comparative Microstructures of Powders and Consolidates of P/M Superalloys Produced by Modern Atomization Processes," R.D. Kissinger and J.K. Tien, Proc. of Third Conference on Rapid Solidification Processing Principles and Technologies (6-8 December 1982).

"Cooling Rates and Fine Microstructures of RSR and AA of SA Powders," F. Cosandey, R.D. Kissinger and J.K. Tien, Proc. 1981 MRS Symposium on Rapidly Solidified Amorphous and Crystalline Alloys, eds. B.H. Kear, B.C. Giessen and M. Cohen, Elsevier Science Publishing, New York, 1982.

B. Presentations

"Hot Workability of an as-HIP P/M Superalloy" J.C. Borofka and J.K. Tien, AIME Annual National Meeting, February, 1985, New York.

END

10-86

DTIC